

Test-Time Degradation Adaption for Open-Set Image Restoration

Yuanbiao Gou¹, Haiyu Zhao¹, Boyun Li¹, Xinyan Xiao², Xi Peng^{1*}

¹College of Computer Science, Sichuan University; ²Baidu Inc.

gouyuanbiao@gmail.com, xiaoxinyan@baidu.com

{haiyuzhao.gm, liboyun.gm, pengx.gm}@gmail.com

Abstract

In contrast to close-set scenarios that restore images from a predefined set of degradations, open-set image restoration aims to handle the unknown degradations that were unforeseen during the pretraining phase, which is less-touched as far as we know. In this work, we explicitly study this challenging problem and reveal its essence, i.e., the unidentified distribution shifts between test and training data. In recent, test-time adaptation emerges as a fundamental method to address this inherent disparities. Inspired by this, we propose a test-time degradation adaption framework for open-set image restoration, which involves three components, i.e., i) a pre-trained and degradation-agnostic diffusion model to generate clean images, ii) a test-time degradation adapter adapts the unknown degradations based on the input image during the testing phase, and iii) the adapter-guided image restoration guides the model through the adapter to produce the corresponding clean image. Through experiments on multiple degradations absent from the training data, we show that our method achieves comparable even better performance than those task-specific methods.

1. Introduction

In recent years, significant advances have been made in the realm of image restoration, and demonstrated remarkable capabilities in addressing a multitude of image degradations [9, 12, 17, 24, 44]. However, a common limitation among most existing methods is their reliance on assumptions rooted in a close-set scenario, i.e., the test degradations closely resemble those encountered during the pre-training phase. This assumption restricts the applicability of these methods to specific types of degradation, hindering their adaptability to a broader range of real-world scenarios where diverse and unforeseen degradations may arise.

To break through the limitation, this study delves into

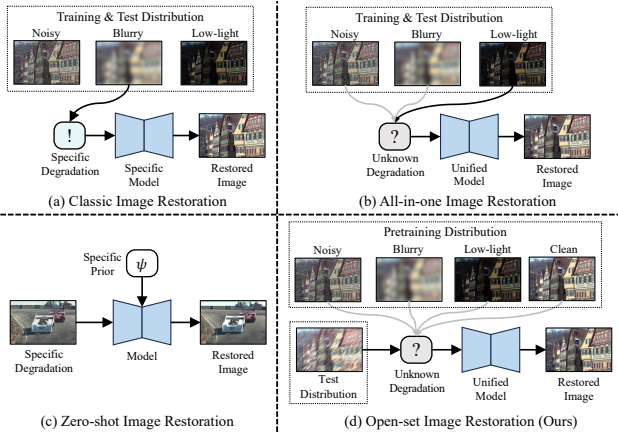


Figure 1. The differences of image restoration (IR) tasks. To be specific, (a) Classic IR works in a close-set scenario where the training and test degradations are the same and known, and customizes a specialized model for each one. (b) All-in-one IR also works in a close-set scenario where the training and test degradations are the same but unknown, and addresses them through a single model. (c) Zero-shot IR focuses on recovery from single degraded sample, which is free from the training degradations, but often suffers from the priors of the test degradations. In contrast, (d) OIR works in a open-set scenario where the test degradations are unknown and different from the pretraining ones. This is analogous to the problem in the realm of natural language processing, which applies the pre-trained Large Language Model to the various downstream tasks not predefined during the pretraining phase.

a more challenging and less-touched problem, i.e., open-set image restoration (OIR). In contrast to conventional close-set approaches, where models only address specific degradations encountered during the pretraining phase, OIR poses a formidable challenge by requiring models to handle unknown degradations absent from the training data. This shift in focus aims to push the boundaries of image restoration, fostering the development of models that exhibit adaptability and resilience in the face of diverse and unexpected degradations. By tackling OIR problem, this work seeks to pave the way for more robust and versatile solutions applicable to complex degradations in the real-world

*Corresponding author

scenarios.

The essence of OIR lies in addressing the challenges posed by real-world scenarios, where the test data may differ significantly from the training data. This could involve variations in degradation types and levels, lighting conditions and so on that were not explicitly covered during the pretraining phase. To tackle this challenge, test-time adaptation (TTA) recently emerges as an effective methodology to address the inherent disparities between test and training data [37]. It adapts the pre-trained model during the testing phase based on the specific characteristics of the test data, allowing the model to perform better on a wider range of input scenarios. This is particularly useful in OIR where the test data may vary from the training data, and the pre-trained model needs to adapt to unknown and unseen degradations for optimal performance.

Building on this inspiration, we present a Test-time degradation Adaption framework for Open-set image restoration, termed TAO, which harnesses the idea of TTA to provide a robust solution for OIR. Specifically, TAO consists of three components, *i.e.*, a pre-trained image diffusion model (PDM), a test-time degradation adapter (TDA), and the adapter-guided image restoration (AIR). In this framework, PDM is adopted as the foundation model for OIR due to the following considerations. First, PDM captures rich knowledges of generating various high-quality visual scenarios, which could be regarded as a generic pretraining for OIR targeting at producing clean images. Second, PDM is degradation-agnostic, and any degradations in test data could be considered as unforeseen. Adapting PDM for OIR during the testing phase has a great potential to pave the way towards universal image restoration system. Note that the testing phase of PDM is referred to the process of image generation, *i.e.*, the step-by-step denoising process.

After each denoising step, TDA and AIR are sequentially conducted for adapting to open-set scenarios and guiding image restoration, respectively. Specifically, TDA employs a learnable adapter during the testing phase for adapting PDM on the test degraded image. This adapter is devised for domain alignment that aligns the generative domain of PDM to the degraded domain of the test image. In this way, the generated image could be translated to the corresponding degraded one, which could be further supervised toward the test degraded image, and in turn updating the generated image. AIR is elaborated to conduct this supervised updating for image restoration. In brief, AIR is inspired by the observation that PDM exhibits an intriguing temporal dynamic [5] during the step-by-step denoising process. Therefore, AIR dynamically and accordingly adjusts the supervision strategies at different denoising steps for achieving a better image restoration.

Overall, the contributions of this work could be summarized as follows.

- To the best of our knowledge, this could be one of the first work that explicitly studies OIR and discovers its essence, *i.e.*, the unidentified distribution shifts between test and training data.
- This work reveals that TTA is an effective methodology for OIR, by adapting the pre-trained model on the test data during the test phase, to address the inherent disparities between test and training data.
- This work presents a test-time degradation adaptation framework for OIR, where two components are devised to adapt open-set scenarios and guide image restoration. Experiments show the effectiveness of this framework.

2. Related Work

In this section, we briefly review recent advances in related topics, which mainly involves test-time adaption, all-in-one image restoration, and zero-shot image restoration.

Test-time Adaption has shown to be effective at tackling distribution shifts between test and training data, by adapting the pre-trained model on test samples. In the past several years, it has gained increasing attention and plentiful methods have been proposed. For example, [37, 42] updated the specific model parameters through the test samples by resorting to the unsupervised objectives. Similarly, [10, 38] aimed to solve the continually changing distribution shifts along the test time. Moreover, [30, 45] considered more challenging and practical adaption settings such as single sample, label shifts, and mixed domain shifts. Besides, [20, 33] shifted their focuses on applications beyond image recognition, such as semantic segmentation and pose estimation.

This work focuses on application of solving OIR through TTA methodologies. In brief, we incorporate PDM with an adapter which is updated for adapting to the test degraded images during the test phase. Besides, we also consider the challenging adaption setting of single test sample.

All-in-one Image Restoration is an emerging problem which has been attracted more and more attentions. Specifically, it aims to address the unknown degradations within a predefined set through one model. For example, [25] firstly studied this problem and proposed to automatically extract the degradation representation from the unknowingly degraded images for assisting the restoration. [31] aimed to encode the degradations' information into prompts, which are then used to dynamically guide the restoration. [17] focused on using the generated text prompts to guide the latent diffusion process for restoring images with unknown degradations. Although remarkable progress has been achieved, they usually need to be trained on a predefined set of degradations, and recover images from the degradations that are unknown but within this set. In other words, they could only be applied to the close-set scenarios.

In contrast, this work is devoted to address OIR prob-

lem, where the test degradations are unknown during the test phase, and meanwhile unforeseen during the pretraining phase. Note that OIR is established on a pre-trained model for image restoration, and adapts it to the downstream tasks (*i.e.*, unknown and unforeseen degradations) during the test phase. Here, we empirically regard the diffusion model [15] as a generic pretraining task for various image restoration tasks.

Zero-shot Image Restoration focuses on recovering the clean image from a single degraded one, without relying on paired clean-degraded images for training. Classic methods are usually devised for specific tasks. For example, [34] performed super resolution by downsampling the low-resolution image to construct the lower-low training pairs. [23] trained dehazing networks by decoupling and coupling the haze image through the physical model of haze formation. Recently, some works focused on methods with more general purpose. For instance, [18, 39] applied the decomposition approaches on the predefined linear degradations, and used the diffusion model to address multiple tasks of image restoration. Similarly, [9] introduced the conditional guidance for eliminating linear or blind degradations through predefined or optimizable linear degradation operators, respectively.

This work is different from the above methods on both the problem and solution. On problem, zero-shot focuses on the restoration from single degraded sample, while open-set focuses on handling the unknown degradations that were unforeseen during the pretraining phase, where the degraded sample does not have to be a single one. On solution, the above methods usually exploit additional degradation priors to assist restoration from single degraded image, while our method only introduces a degradation-agnostic adapter for all unknown and unforeseen degradations.

3. The Proposed Method

In this section, we first briefly retrospect the preliminary knowledge of PDM, and then progressively illustrate the proposed TAO, TDA and AIR.

3.1. Preliminary

Given a data distribution $x_0 \sim q(x_0)$ and a noise distribution $x_T \sim \mathcal{N}(0, I)$, the diffusion model [15] defines a T -timestep diffusion process, which corrupts x_0 to x_T by sequentially adding the random noise $\epsilon \sim \mathcal{N}(0, I)$, and a T -timestep denoising process, which recovers x_T to x_0 by progressively removing the noise ϵ . Importantly, there is an elegant property in the diffusion process, *i.e.*,

$$x_t = \sqrt{\bar{\alpha}_t}x_0 + \sqrt{1 - \bar{\alpha}_t}\epsilon, \quad (1)$$

where $t \in \{0, \dots, T\}$, $\bar{\alpha}_t = \prod_{i=0}^t \alpha_i$, $\alpha_i = 1 - \beta_i$ and β_i is the variance of the i th timestep. Through this formula, the

diffusion model learns a denoiser for the denoising process via the following objectives, *i.e.*,

$$\nabla_{\theta} \parallel \epsilon - \mathcal{Z}_{\theta}(\sqrt{\bar{\alpha}_t}x_0 + \sqrt{1 - \bar{\alpha}_t}\epsilon, t) \parallel, \quad (2)$$

where \mathcal{Z}_{θ} is the denoising network, and t is randomly sampled during the training phase. For a well-trained diffusion model, denoising process progressively yields x_{t-1} from x_t in terms of $\epsilon_t = \mathcal{Z}_{\theta}(x_t, t)$ until $t = 0$. According to Bayes Theorem, x_{t-1} could be sampled through the following process, *i.e.*,

$$\begin{aligned} q(x_{t-1}|x_t) &= \mathcal{N}(x_{t-1}; \mu(x_t, \hat{x}_0), \tilde{\beta}_t), \\ \mu(x_t, \hat{x}_0) &= \frac{\sqrt{\bar{\alpha}_{t-1}}\beta_t \hat{x}_0 + \sqrt{\alpha_t}(1 - \bar{\alpha}_{t-1})x_t}{1 - \bar{\alpha}_t}, \\ \hat{x}_0 &= \frac{x_t - \sqrt{1 - \bar{\alpha}_t}\epsilon_t}{\sqrt{\bar{\alpha}_t}}, \quad \tilde{\beta}_t = \frac{1 - \bar{\alpha}_{t-1}}{1 - \bar{\alpha}_t}\beta_t, \end{aligned} \quad (3)$$

where \hat{x}_0 is the estimated output of x_t in terms of Eq.(1). To guide x_{t-1} towards the desired output x_0 , the conditional guidance y could be introduced through the following formula [8, 9], *i.e.*,

$$q(x_{t-1}|x_t, y) \propto N(x_{t-1}; \mu(x_t, \hat{x}_0) + s\mathcal{G}, \tilde{\beta}_t), \quad (4)$$

where s is the scale of guidance, $\mathcal{G} = \nabla_{\hat{x}_0} \log p_{\phi}(y|\hat{x}_0)$, and $p_{\phi}(\cdot)$ is a model bridging the gaps between \hat{x}_0 and y . For image restoration, the test degraded image is introduced as the y , and the x_0 is the desired clean output.

3.2. The Framework of TAO

To endow PDM with the capacity of OIR, the key lies in implementing $p_{\phi}(\cdot)$ to produce appropriate guidance of gradients \mathcal{G} , towards the clean version x_0 of the test degraded image y . In this work, $p_{\phi}(\cdot)$ is implemented through two components, *i.e.*, TDA and AIR, which are devised for open-set scenarios and image restoration, respectively. To address the challenges posed by open-set scenarios, TDA introduces a degradation-agnostic adapter during the test phase (*i.e.*, denoising process of PDM) for adapting PDM to the unknown and unforeseen degradations. The adapter is implemented by a simple neural network, and optimized once at each denoising timestep towards aligning the domain of generated images to that of the test degraded image. As a result, the generated images could be translated to the corresponding degraded ones, which could be further supervised towards the y , and in turn produce \mathcal{G} to update the generated images towards the desired x_0 . AIR is elaborated to conduct this supervised process for image restoration. Specifically, AIR is inspired by the observation that PDM exhibits an intriguing temporal dynamic during the denoising process, *i.e.*, images are generated from the unrecognizable contents to the perceptually rich contents, and finally the imperceptible details. Therefore, AIR dynamically adjusts the supervision strategies by gradually shifting the focuses from high- to low-level contents during the denoising process.

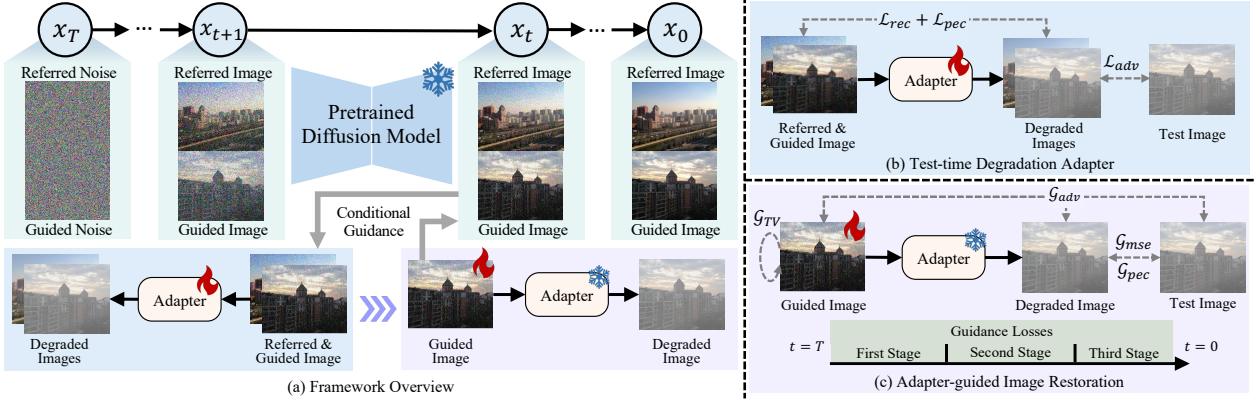


Figure 2. Overview of the proposed TAO, which addresses OIR by exploiting i) a PDM as the generic pre-trained model for various tasks of image restoration, and at each step of denoising alternatively performing ii) a TDA for adapting to the unknown and unseen degradations posed by open-set scenario, and iii) an AIR for guiding the PDM through the TDA to restore the desired clean images.

The framework of TAO is illustrated in Fig.2, where an PDM is frozen to progressively denoising the pure noise x_T to the clean image x_0 . For a given degraded image y , TAO first samples two maps of random noise at $t = T$, and thus two images will be generated at each timestep. Here, we refer to the image guided towards the clean version of the y as the guided image x_t^g , and the other unguided one as the referred image x_t^r . The introduction of x_t^r is for preventing TDA from falling into trivial solutions, and assisting AIR to guide x_t^g towards the desired clean image x_0^g . At each timestep t , the images x_t^g , x_t^r , and y are first fed into TDA for optimizing the adapter ϕ through the objectives of domain alignment, and then sent into AIR for updating x_t^g towards x_0^g , which best matches the y undergoing the ϕ , through the conditional guidance in Eq.(4).

3.3. Test-time Degradation Adapter

The essence of OIR lies in addressing the unidentified distribution shifts between test and training data, while TTA recently emerges as an effective methodology to address this inherent disparities. With the motivations, TDA is presented for adapting PDM to the downstream shifted distribution of degradations during the test phase.

TDA employs a four-layer convolution neural network as the adapter ϕ , which is optimized for aligning the domain of generated images \hat{x}_0^g , \hat{x}_0^r to that of the test degraded image y . Note that \hat{x}_0^g , \hat{x}_0^r are the estimated output of x_t^g , x_t^r , respectively. To this end, we introduce adversarial training which has shown to be effective in aligning the source and target domains, and the translated samples usually capture rich visual characteristics inherent to the target domain. Therefore, TDA aligns $\phi([\hat{x}_0^g, \hat{x}_0^r])$ to y which involves significant degradations through

$$\mathcal{L}_{adv} = \log(1 - \mathcal{D}(\phi([\hat{x}_0^g, \hat{x}_0^r])), \quad (5)$$

where $[\cdot]$ denotes the concatenation along the dimension of

batch size, and \mathcal{D} is a discriminator optimized through

$$\mathcal{L}_{dis} = -\log \mathcal{D}([y, y]) - \log(1 - \mathcal{D}(\phi([\hat{x}_0^g, \hat{x}_0^r])). \quad (6)$$

Meanwhile, TDA introduces a reconstruction loss to maintain the content consistency before and after alignment, *i.e.*,

$$\mathcal{L}_{rec} = \|\hat{x}_0^g, \hat{x}_0^r - \phi([\hat{x}_0^g, \hat{x}_0^r])\|_2^2. \quad (7)$$

Besides, the perceptual loss is adopted to remain the semantic consistency before and after alignment, *i.e.*,

$$\mathcal{L}_{pec} = \|\mathcal{V}([\hat{x}_0^g, \hat{x}_0^r]) - \mathcal{V}(\phi([\hat{x}_0^g, \hat{x}_0^r]))\|_2^2, \quad (8)$$

where $\mathcal{V}(\cdot)$ denotes the feature maps extracted from the pre-trained VGG network. Overall, the objective for optimizing the adapter ϕ is

$$\mathcal{L}_\phi = \lambda_1 * \mathcal{L}_{rec} + \lambda_2 * \mathcal{L}_{pec} + \lambda_3 * \mathcal{L}_{adv}, \quad (9)$$

where λ_1 , λ_2 , and λ_3 are the optimization weights. Through iterative optimizations during the denoising process, ϕ progressively translate \hat{x}_0^g , \hat{x}_0^r to the domain of y . Note that \hat{x}_0^r is introduced to prevent ϕ from the trivial solution of identity mapping.

3.4. Adapter-guided Image Restoration

With the adapter ϕ , \hat{x}_0^g could be translated to the degraded domain of y through $\phi(\hat{x}_0^g)$, which could be further supervised towards the y , and in turn produce \mathcal{G} to update the generated images \hat{x}_0^g to the desired clean output x_0^g . AIR is devised to perform this supervised updating process.

Existing studies [5] have shown that the denoising process exhibits an intriguing temporal dynamic, *i.e.*, \hat{x}_0^g is generated from the unrecognizable contents to the perceptually rich contents, and finally the imperceptible details. In other words, the contents to be restored are varying as

the timesteps during the denoising process. To take full advantages of PDM, AIR empirically divides the denoising process into three stages, and guides the restoration through different strategies at different stages.

In the first stage where $t \sim T$, the images have a lower signal-to-noise ratio, where the contents are unrecognizable and only contains some global information such as colors, layouts distributed throughout image. Therefore, AIR applied mse loss on the spatial pixels and color channels, *i.e.*,

$$\mathcal{G} = \gamma_1 * \nabla_{\hat{x}_0} \| y - \phi(\hat{x}_0) \|_2^2, \quad (10)$$

where γ_1 is the loss weight, \hat{x}_0 is the estimated output of $x_t \in \{x_t^g, x_t^r\}$. AIR also use this guidance on the referred image x_t^r so that it embraces similar global properties as the y , since it is beneficial to the optimization of adapter. Besides, a linear warmup is adopted on γ_1 .

In the second stage where $t \sim T/2$, PDM prefers to generate the perceptually rich contents, and thus AIR focuses more on restoring the perceptual contents of y . To this end, the perceptual loss is adopted, *i.e.*,

$$\mathcal{G}_{pec} = \nabla_{\hat{x}_0^g} \| \mathcal{V}(y) - \mathcal{V}(\phi(\hat{x}_0^g)) \|_2^2. \quad (11)$$

Meanwhile, the adversarial loss is also introduced to boost the perceptual quality, *i.e.*,

$$\begin{aligned} \mathcal{G}_{adv} &= \nabla_{\hat{x}_0^g} \log(1 - \mathcal{D}(\hat{x}_0^g - y)) \\ \mathcal{L}_{dis} &= -\log(1 - \mathcal{D}(\hat{x}_0^g - y)) \\ &\quad - \log \mathcal{D}([\hat{x}_0^g, \hat{x}_0^r] - \phi([\hat{x}_0^g, \hat{x}_0^r])). \end{aligned} \quad (12)$$

Through this loss, \hat{x}_0^g will be further updated toward the clean image whose degraded version matches y , by aligning the distribution of information loss. Besides, the mse loss is also employed to remain the global contents, *i.e.*,

$$\mathcal{G}_{mse} = \nabla_{\hat{x}_0^g} \| y - \phi(\hat{x}_0^g) \|_2^2. \quad (13)$$

Overall, the guidance loss for the second stage is

$$\mathcal{G} = \gamma_2 * \mathcal{G}_{mse} + \gamma_3 * \mathcal{G}_{pec} + \gamma_4 * \mathcal{G}_{adv}, \quad (14)$$

where γ_{2-4} are the loss weights.

In the third stage where $t \sim 0$, the perceptually rich contents are already prepared in \hat{x}_0^g , AIR only required to recover the imperceptible details. In other words, \hat{x}_0^g is very close to the natural image, and thus some extra priors could be introduced to regulate the final output. In consideration of generality, we only introduce the total variation loss, *i.e.*, $\mathcal{G} = \gamma_5 * TVLoss(\hat{x}_0^g)$, where γ_5 is the loss weight. Note that although the third stage mainly affects the imperceptible details, the pixel values still fluctuate, and thus the guidance in the second stage is still used for a better numerical fidelity.

4. Experiments

In this section, we first introduce the experimental settings, and then show quantitative and qualitative results on multiple degradations. Finally, we perform analysis experiments including ablation studies and result visualizations.

4.1. Experimental Settings

To evaluate the effectiveness of TAO on addressing OIR, we conduct experiments on multiple tasks of image restoration with exactly the same settings, except for the loss weights ($\lambda_{1-3}, \gamma_{1-5}$) and the scale of guidance s , which are fine-tuned for different types of degradation to obtain the best results. In experiments, we employ an unconditional image diffusion model [8] pretrained on ImageNet [7] as PDM, and sets the timestep as $T = 1000$, which is further divided into three stages in a heuristic way, *i.e.*, the first stage 999-600, the second stage 600-50, and the third stage 50-0. Since PDM is pre-trained on large-scale nature images for high-quality image generation, any degradation in the test image could be regarded as the unforeseen. Both the adapter and discriminators are four-layer convolutional networks, and optimized once at each denoising timestep through Adam optimizer with default learning rate of 1e-3. The first nine layers of pretrained VGG-16 [35] network are used to extract the semantic feature maps for calculating the perceptual loss. For evaluation, considering the specificity of our methods, *i.e.*, adaption on single test sample, we mainly compare it with those task-specific zero-shot methods, and some classic learning-based methods. To access their performance, PSNR and SSIM metrics are employed, and all experiments are conducted through PyTorch framework on Ubuntu20.04 with GeForce RTX 3090 GPUs.

4.2. Experimental Results

In this section, we evaluate our method on image restoration tasks of image dehazing, low-light image enhancement, and image denoising.

Image Dehazing aims to remove the haze and boost the visibility of hazy image, which has spawned many methods in the past decades. In experiments, we introduce HSTS dataset from RESIDE [22] for evaluations. To be specific, RESIDE is a large scale haze image dataset, and HSTS is one of the test subsets, which contains 10 synthetic and 10 real-world hazy images. Before the evaluation, we first center crop the images along the shorter edge, and then resize them to match the image size of the PDM.

For comprehensive comparisons, we compare TAO with 10 representative methods, which are specially designed for image dehazing, and could be roughly divided into two groups, *i.e.*, classic learning-based and zero-shot methods. Specifically, the classic learning-based methods are DehazeNet (DEN) [3], MSCNN (MSN) [32], AOD-Net

Table 1. Quantitative results of image dehazing on HSTS from RESIDE dataset. Our method outperforms the zero-shot methods, and obtains comparable results with the classic methods through supervised learning.

Metrics	Classic Learning Methods				Zero-shot Methods					OIR	
	DEN	MSN	AOD	CAP	DCP	BCCR	GRM	NLD	DDIP	YOLY	
PSNR \uparrow	23.96	18.40	19.15	21.69	18.42	15.75	17.41	18.18	18.22	21.24	21.38
SSIM \uparrow	0.902	0.826	0.860	0.868	0.854	0.783	0.833	0.814	0.832	0.835	0.859

Table 2. Quantitative results of low-light image enhancement on LOL dataset. Our method obtains the best SSIM values and the second PSNR values in the zero-shot methods, and only the classic learning-based MBLLEN outperforms our method on both the two metrics.

Metrics	Classic Learning Methods				Zero-shot Methods					OIR
	LNet	RNet	MBLLEN	EGAN	ExCNet	ZDCE	ZDCE+	RRDN	GDP	
PSNR \uparrow	13.39	17.87	18.03	14.85	17.15	15.33	15.71	11.24	15.75	16.28
SSIM \uparrow	0.623	0.699	0.809	0.815	0.720	0.763	0.765	0.543	0.665	0.766

Table 3. Quantitative results of image denoising on Kodak dataset. N.I. denotes the noise images. From the table, one could see that our method is comparable to even better than those zero-shot image denoising methods.

Metrics	N.I.	BM3D	N2S	N2V	DIP	Ours
PSNR \uparrow	26.35	28.63	28.71	27.17	27.58	28.17
SSIM \uparrow	0.757	0.795	0.864	0.846	0.808	0.827

(AOD) [21], and CAP [47]. The zero-shot methods are DCP [14], BCCR [29], GRM [4], NLD [2], DDIP [11] and YOLY [24].

The quantitative results are presented in Tab.1, from which one could see that our method achieves comparable even better results than those task-specific methods. To be specific, our method obtains the best performance in zero-shot methods, and outperforms YOLY and DCP with 0.14/0.024 and 2.96/0.005 in PSNR/SSIM metrics, respectively. Meanwhile, even compared to the classic learning-based methods, our method still outperforms some of them, and achieves comparable performance with the other. For instance, our method obtains 2.98/0.033 higher PSNR/SSIM value than MSN, 2.23 higher PSNR value than AOD. Although it is lower than CAP and DEN, the performance gaps are not huge, *e.g.*, 0.31/0.009 lower than CAP and 2.58/0.043 lower than DEN in PSNR/SSIM metrics. In addition, we show and analyze their qualitative results in Fig.3, which show that our method achieves better fidelity and realness.

Low-light Image Enhancement aims at improving the perception of the image captured in the environment with poor illumination. To evaluate our method on this challenge task, we introduce the test subset from LOL [41] dataset.

LOL includes 485 training and 15 test image pairs of low- and normal-light, which contain noises produced during the photo capture process. Since the images have a resolution of 400 \times 600, we first center crop the image along the shorter edges, and then resize them to be applicable to the PDM.

For comprehensive comparisons, we compare our method with nine low-light image enhancement methods, which are divided into two categories, *i.e.*, classical learning-based and zero-shot methods. To be specific, the classical learning-based methods are Lighten-Net (LNet) [26], Retinex-Net (RNet) [40], MBLLEN [28], and EnlightenGAN (EGAN) [16]. The zero-shot methods are ExCNet [43], Zero-DCE (ZDEC) [13], Zero-DCE++ (ZDEC+) [27], RRDNet (RRDN) [46], and GDP [9]. The above methods except GDP are specially designed for low-light image enhancement, while our method is devised for more general purpose of OIR, and the only difference for different tasks lies in the loss weights and the guidance scale.

The quantitative results are shown in Tab.2. From the Table, one could see that our method achieves comparable even better results than those specific-designed methods. In the zero-shot methods, our method obtains the best and the second performance in terms of SSIM and PSNR metrics, respectively. In PSNR metric, our method outperforms the other methods except ExCNet with the margin of 0.53-5.04. Although ExCNet achieves the better PSNR value, our method achieves the best SSIM values and exceeds it with a margin of 0.046. Besides, even compared to the classic learning-based methods, our method is competitive and obtains better results than some of them. For instance, our method obtains 2.89/0.143 higher PSNR/SSIM value than LNet, 1.43 higher PSNR value than EGAN, and 0.067 higher SSIM value than RNet. Only the MBLLEN



Figure 3. Qualitative results of image dehazing, from which one could see that existing methods excessively dehazing resulting in darkening and/or artifacting of the image. In contrast, our method obtains clearer results which are closer to the natural ground truth.

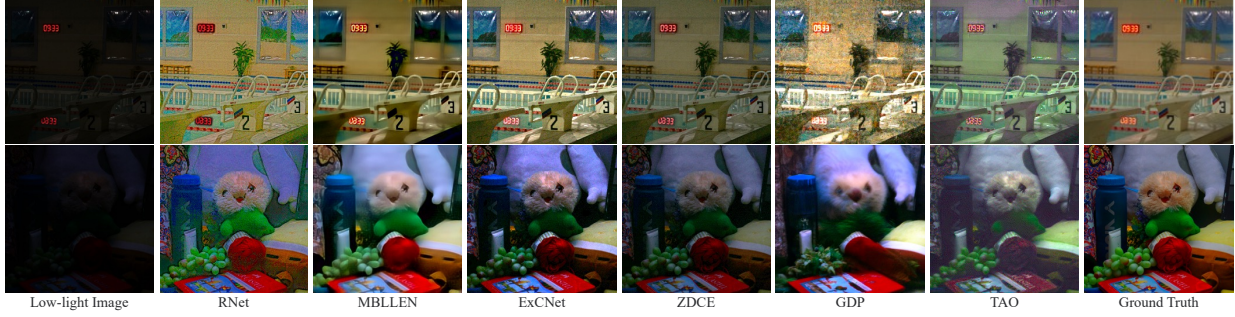


Figure 4. Qualitative results of low-light image enhancement, from which one could see that our results are not as smooth as the MBLLEN nor as dark as ZDEC. Although there is a slight color bias from the ground truth, it achieves a rational lighting of the dark images.

could outperform our method on both the PSNR and SSIM metrics. Moreover, we present and analyze the qualitative results in Fig.4, which demonstrate our method enlightens the dark images reliably and reasonably.

Image Denoising aims to remove noises from an noise image. To evaluate our method, we introduce Kodak24 dataset which consists of 24 natural clean images, and is commonly used for testing image denoising methods. Similarly, we center crop and resize the image to match the size of the PDM, and obtain the noise images by adding the Gaussian noises with the noise level of $\sigma = 30$ to the clean images.

We compare our method with four zero-shot image denoising methods, *i.e.*, BM3D [6], N2S [1], N2V [19], and DIP [36]. The above methods except for DIP are specially designed for image denoising. The quantitative results are presented in Tab.3. From the table, one could see that our method obtains comparable even better results than those task-specific methods. To be specific, our method obtains 0.032 and 0.019 higher SSIM value than BM3D and DIP, respectively. Meanwhile, our method also outperforms N2V and DIP in PSNR value with a large margin of 1.00 and 0.59, respectively. Although not achieving the best performance, our method enjoys the appealing capacity of addressing OIR in one model. In addition, we present the qualitative results in Fig.5, from which one could see that

our method obtains clearer results with better fidelity to ground truths than the compared methods.

4.3. Analysis Experiments

In this section, we conduct analysis experiments w.r.t. our proposed TDA and AIR mainly on image dehazing.

The effectiveness of TDA. Since PDM cannot achieve image dehazing without TDA, we show its effectiveness by observing whether it aligns the domain of generated images to that of the degraded image after the optimization during the denoising process. The results are presented in Fig.6, from which one could observe that TDA aligns the domain of generated images well with that of the degraded images. For example, the haze in the top row is uneven distributed in the test degraded image, and the same effect exists in the degraded referred/guided image. Besides, in the bottom row, the degree of darkness in the degraded referred/guided image is similar to that in the test degraded image. Overall, our TDA exhibits significant capability of domain alignment to the unknown and unseen degradations.

The effectiveness of AIR. Here, we first demonstrate the rationality of TDG in Fig.7, which exhibits a typical denoising process of the PDM, from which one could see the significant temporal dynamics, *i.e.*, the images are generated from the unrecognizable contents to the perceptually rich contents, and finally the imperceptible details. These



Figure 5. Qualitative results on image denoising, from which one could observe that existing methods excessively denoising resulting in smoothing and/or artifacting of the images. In contrast, our method obtains clearer and sharper results which are closer to ground truths.

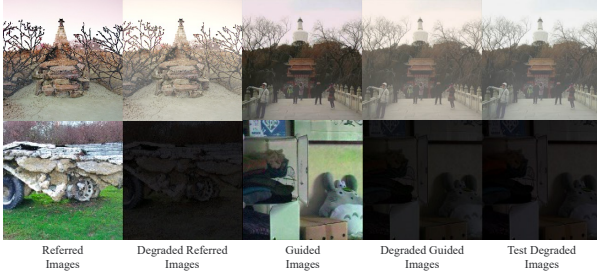


Figure 6. The visualizations w.r.t TDA, where the Referred/Guided Images are translated to Degraded Referred/Guided Images by TDA, whose domains align well with that of Test Degraded Images.

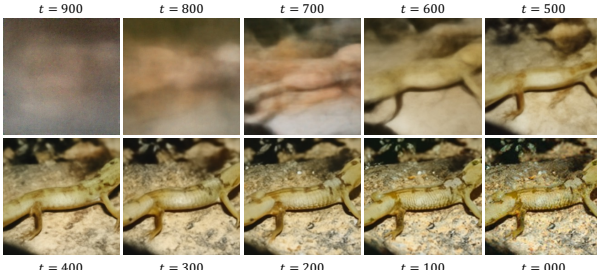


Figure 7. The temporal dynamics of PDM during the denoising process, which motivates our AIR to guide the image restoration through different strategies at different denoising steps.

Table 4. Ablation studies on AIR, where U.G. denotes using the same guidance loss of mean squared error throughout the denoising process. -F.S., -S.S., and -T.S. receptively denote to remove the First Stage, Second Stage, and Third Stage in AIR, using only the above U.G.. The results demonstrate the indispensable roles of the three stages for image dehazing.

Metrics	U.G.	-F.S.	-S.S.	-T.G.	TDG
PSNR \uparrow	20.42	20.22	20.43	21.13	21.38
SSIM \uparrow	0.851	0.857	0.837	0.857	0.859

dynamics also imply the varying of the contents should be focused and restored in the test degraded image, and thus applying different guidance strategies could facilitate the image restoration. Besides, we present the results of ablation studies on AIR in Tab.4, which demonstrate the effectiveness of our designs on facilitating the image dehazing.

5. Conclusion

This paper explicitly explores the challenges posed by open-set scenarios, and formally defines the problem of open-set image restoration. To solve this problem, this work reveals its essence from the perspective of distribution shifts, and discovers the methodology of test-time adaption is adept at addressing this inherent disparities. Motivated by this, this work presented a test-time degradation adaptation framework for open-set image restoration, which is ingenious in following ways. First, It considers a pre-trained image diffusion model as the general pretraining model for solving various tasks of image restoration. Then, it introduces an adapter optimized during the test phase for adapting the pre-trained model to the unknown and unseen test degradations. Finally, it dynamically adjusts the guidance strategies following the denoising process to obtain a better restoration result. Through experiments on multiple degradations, this work demonstrate the effectiveness of the proposed method.

Potential Broader Impact

This paper considers a novel problem in Image Restoration that restores the clean images from the degraded ones under an open-set scenario. Although there are potential societal consequences of this work, none which we feel serious and must be specifically highlighted here. For example, the most serious cases may be the recovery of images that have been intentionally damaged by someone else, or do not match the facts affecting the decisions made on that.

References

[1] Joshua Batson and Loic Royer. Noise2self: Blind denoising by self-supervision. In *International Conference on Machine Learning*, pages 524–533, 2019. 7

[2] Dana Berman, Shai Avidan, et al. Non-local image dehazing. In *Proceedings of the IEEE/CVF Conference on Computer Vision and Pattern Recognition*, pages 1674–1682, 2016. 6

[3] Bolun Cai, Xiangmin Xu, Kui Jia, Chunmei Qing, and Dacheng Tao. Dehazenet: An end-to-end system for single image haze removal. *IEEE Transactions on Image Processing*, 25(11):5187–5198, 2016. 5

[4] Chen Chen, Minh N Do, and Jue Wang. Robust image and video dehazing with visual artifact suppression via gradient residual minimization. In *European Conference on Computer Vision*, pages 576–591, 2016. 6

[5] Jooyoung Choi, Jungbeom Lee, Chaehun Shin, Sungwon Kim, Hyunwoo Kim, and Sungroh Yoon. Perception prioritized training of diffusion models. In *Proceedings of the IEEE/CVF Conference on Computer Vision and Pattern Recognition*, pages 11472–11481, 2022. 2, 4

[6] Kostadin Dabov, Alessandro Foi, Vladimir Katkovnik, and Karen Egiazarian. Image denoising by sparse 3-d transform-domain collaborative filtering. *IEEE Transactions on Image Processing*, 16(8):2080–2095, 2007. 7

[7] Jia Deng, Wei Dong, Richard Socher, Li-Jia Li, Kai Li, and Li Fei-Fei. Imagenet: A large-scale hierarchical image database. In *Proceedings of the IEEE/CVF Conference on Computer Vision and Pattern Recognition*, pages 248–255, 2009. 5

[8] Prafulla Dhariwal and Alexander Nichol. Diffusion models beat gans on image synthesis. *Advances in Neural Information Processing Systems*, 34:8780–8794, 2021. 3, 5

[9] Ben Fei, Zhaoyang Lyu, Liang Pan, Junzhe Zhang, Weidong Yang, Tianyue Luo, Bo Zhang, and Bo Dai. Generative diffusion prior for unified image restoration and enhancement. In *Proceedings of the IEEE/CVF Conference on Computer Vision and Pattern Recognition*, pages 9935–9946, 2023. 1, 3, 6

[10] Yulu Gan, Yan Bai, Yihang Lou, Xianzheng Ma, Renrui Zhang, Nian Shi, and Lin Luo. Decorate the newcomers: Visual domain prompt for continual test time adaptation. In *Proceedings of the AAAI Conference on Artificial Intelligence*, pages 7595–7603, 2023. 2

[11] Yosef Ganelsman, Assaf Shocher, and Michal Irani. “double-dip”: unsupervised image decomposition via coupled deep-image-priors. In *Proceedings of the IEEE/CVF Conference on Computer Vision and Pattern Recognition*, pages 11026–11035, 2019. 6

[12] Yuanbiao Gou, Peng Hu, Jiancheng Lv, Joey Tianyi Zhou, and Xi Peng. Multi-scale adaptive network for single image denoising. *Advances in Neural Information Processing Systems*, 35:14099–14112, 2022. 1

[13] Chunle Guo, Chongyi Li, Jichang Guo, Chen Change Loy, Junhui Hou, Sam Kwong, and Runmin Cong. Zero-reference deep curve estimation for low-light image enhancement. In *Proceedings of the IEEE/CVF Conference on Computer Vision and Pattern Recognition*, pages 1780–1789, 2020. 6

[14] Kaiming He, Jian Sun, and Xiaoou Tang. Single image haze removal using dark channel prior. *IEEE Transactions on Pattern Analysis and Machine Intelligence*, 33(12):2341–2353, 2010. 6

[15] Jonathan Ho, Ajay Jain, and Pieter Abbeel. Denoising diffusion probabilistic models. *Advances in Neural Information Processing Systems*, 33:6840–6851, 2020. 3

[16] Yifan Jiang, Xinyu Gong, Ding Liu, Yu Cheng, Chen Fang, Xiaohui Shen, Jianchao Yang, Pan Zhou, and Zhangyang Wang. Enlightengan: Deep light enhancement without paired supervision. *IEEE Transactions on Image Processing*, 30:2340–2349, 2021. 6

[17] Yitong Jiang, Zhaoyang Zhang, Tianfan Xue, and Jinwei Gu. Autodir: Automatic all-in-one image restoration with latent diffusion. *arXiv preprint arXiv:2310.10123*, 2023. 1, 2

[18] Bahjat Kawar, Michael Elad, Stefano Ermon, and Jiaming Song. Denoising diffusion restoration models. *Advances in Neural Information Processing Systems*, 35:23593–23606, 2022. 3

[19] Alexander Krull, Tim-Oliver Buchholz, and Florian Jug. Noise2void-learning denoising from single noisy images. In *Proceedings of the IEEE/CVF Conference on Computer Vision and Pattern Recognition*, pages 2129–2137, 2019. 7

[20] Taeyeop Lee, Jonathan Tremblay, Valts Blukis, Bowen Wen, Byeong-Uk Lee, Inkyu Shin, Stan Birchfield, In So Kweon, and Kuk-Jin Yoon. Tta-cope: Test-time adaptation for category-level object pose estimation. In *Proceedings of the IEEE/CVF Conference on Computer Vision and Pattern Recognition*, pages 21285–21295, 2023. 2

[21] Boyi Li, Xulian Peng, Zhangyang Wang, Jizheng Xu, and Dan Feng. Aod-net: All-in-one dehazing network. In *Proceedings of the IEEE International Conference on Computer Vision*, pages 4770–4778, 2017. 6

[22] Boyi Li, Wenqi Ren, Dengpan Fu, Dacheng Tao, Dan Feng, Wenjun Zeng, and Zhangyang Wang. Benchmarking single-image dehazing and beyond. *IEEE Transactions on Image Processing*, 28(1):492–505, 2018. 5

[23] Boyun Li, Yuanbiao Gou, Shuhang Gu, Jerry Zitao Liu, Joey Tianyi Zhou, and Xi Peng. You only look yourself: Unsupervised and untrained single image dehazing neural network. *International Journal of Computer Vision*, 129:1754–1767, 2021. 3

[24] Boyun Li, Yuanbiao Gou, Shuhang Gu, Jerry Zitao Liu, Joey Tianyi Zhou, and Xi Peng. You only look yourself: Unsupervised and untrained single image dehazing neural network. *International Journal of Computer Vision*, 129:1754–1767, 2021. 1, 6

[25] Boyun Li, Xiao Liu, Peng Hu, Zhongqin Wu, Jiancheng Lv, and Xi Peng. All-in-one image restoration for unknown corruption. In *Proceedings of the IEEE/CVF Conference on Computer Vision and Pattern Recognition*, pages 17452–17462, 2022. 2

[26] Chongyi Li, Jichang Guo, Fatih Porikli, and Yanwei Pang. Lightennet: A convolutional neural network for weakly illuminated image enhancement. *Pattern Recognition Letters*, 104:15–22, 2018. 6

[27] Chongyi Li, Chunle Guo, and Chen Change Loy. Learning to enhance low-light image via zero-reference deep curve estimation. *IEEE Transactions on Pattern Analysis and Machine Intelligence*, 44(8):4225–4238, 2021. 6

[28] Feifan Lv, Feng Lu, Jianhua Wu, and Chongsoon Lim. Mbllen: Low-light image/video enhancement using cnns. In *BMVC*, page 4, 2018. 6

[29] Gaofeng Meng, Ying Wang, Jiangyong Duan, Shiming Xiang, and Chunhong Pan. Efficient image dehazing with boundary constraint and contextual regularization. In *Proceedings of the IEEE International Conference on Computer Vision*, pages 617–624, 2013. 6

[30] Shuaicheng Niu, Jiaxiang Wu, Yifan Zhang, Zhiqian Wen, Yaofo Chen, Peilin Zhao, and Mingkui Tan. Towards stable test-time adaptation in dynamic wild world. *arXiv preprint arXiv:2302.12400*, 2023. 2

[31] Vaishnav Potlapalli, Syed Waqas Zamir, Salman Khan, and Fahad Shahbaz Khan. Promptir: Prompting for all-in-one blind image restoration. *arXiv preprint arXiv:2306.13090*, 2023. 2

[32] Wenqi Ren, Si Liu, Hua Zhang, Jinshan Pan, Xiaochun Cao, and Ming-Hsuan Yang. Single image dehazing via multi-scale convolutional neural networks. In *European Conference on Computer Vision*, pages 154–169, 2016. 5

[33] Inkyu Shin, Yi-Hsuan Tsai, Bingbing Zhuang, Samuel Schulter, Buyu Liu, Sparsh Garg, In So Kweon, and Kuk-Jin Yoon. Mm-tta: multi-modal test-time adaptation for 3d semantic segmentation. In *Proceedings of the IEEE/CVF Conference on Computer Vision and Pattern Recognition*, pages 16928–16937, 2022. 2

[34] Assaf Shocher, Nadav Cohen, and Michal Irani. Zero-shot super-resolution using deep internal learning. In *Proceedings of the IEEE/CVF Conference on Computer Vision and Pattern Recognition*, pages 3118–3126, 2018. 3

[35] Karen Simonyan and Andrew Zisserman. Very deep convolutional networks for large-scale image recognition. *arXiv preprint arXiv:1409.1556*, 2014. 5

[36] Dmitry Ulyanov, Andrea Vedaldi, and Victor Lempitsky. Deep image prior. In *Proceedings of the IEEE/CVF Conference on Computer Vision and Pattern Recognition*, pages 9446–9454, 2018. 7

[37] Dequan Wang, Evan Shelhamer, Shaoteng Liu, Bruno Olshausen, and Trevor Darrell. Tent: Fully test-time adaptation by entropy minimization. In *Proceedings of the International Conference on Learning Representations*, 2021. 2

[38] Qin Wang, Olga Fink, Luc Van Gool, and Dengxin Dai. Continual test-time domain adaptation. In *Proceedings of the IEEE/CVF Conference on Computer Vision and Pattern Recognition*, pages 7201–7211, 2022. 2

[39] Yinhuai Wang, Jiwen Yu, and Jian Zhang. Zero-shot image restoration using denoising diffusion null-space model. *Proceedings of the International Conference on Learning Representations*, 2022. 3

[40] Chen Wei, Wenjing Wang, Wenhan Yang, and Jiaying Liu. Deep retinex decomposition for low-light enhancement. *arXiv preprint arXiv:1808.04560*, 2018. 6

[41] Chen Wei, Wenjing Wang, Wenhan Yang, and Jiaying Liu. Deep retinex decomposition for low-light enhancement. *arXiv preprint arXiv:1808.04560*, 2018. 6

[42] Mouxing Yang, Yunfan Li, Zhang Changqing, Peng Hu, and Xi Peng. Test-time adaption against multi-modal reliability bias. In *Proceedings of the International Conference on Learning Representations*, 2024. 2

[43] Lin Zhang, Lijun Zhang, Xiao Liu, Ying Shen, Shaoming Zhang, and Shengjie Zhao. Zero-shot restoration of backlit images using deep internal learning. In *Proceedings of the 27th ACM international conference on multimedia*, pages 1623–1631, 2019. 6

[44] Haiyu Zhao, Yuanbiao Gou, Boyun Li, Dezhong Peng, Jiancheng Lv, and Xi Peng. Comprehensive and delicate: An efficient transformer for image restoration. In *Proceedings of the IEEE/CVF Conference on Computer Vision and Pattern Recognition*, pages 14122–14132, 2023. 1

[45] Zhi Zhou, Lan-Zhe Guo, Lin-Han Jia, Dingchu Zhang, and Yu-Feng Li. Ods: test-time adaptation in the presence of open-world data shift. In *International Conference on Machine Learning*, pages 42574–42588. PMLR, 2023. 2

[46] Anqi Zhu, Lin Zhang, Ying Shen, Yong Ma, Shengjie Zhao, and Yicong Zhou. Zero-shot restoration of underexposed images via robust retinex decomposition. In *2020 IEEE International Conference on Multimedia and Expo (ICME)*, pages 1–6, 2020. 6

[47] Qingsong Zhu, Jiaming Mai, and Ling Shao. A fast single image haze removal algorithm using color attenuation prior. *IEEE Transactions on Image Processing*, 24(11):3522–3533, 2015. 6